Effect of Magnetic Fields on Resonant Solar Acoustic Frequencies

TUNEER CHAKRABORTY

Advisor: Prof. Shravan M Hanasoge

Department of Astronomy and Astrophysics
Tata Institute of Fundamental Research

Submitted in partial fulfilment of the requirement for the degree of
Master of Science

TIFR, Mumbai July 2019

Declaration

I hereby declare that except where specific reference is made to the work of others, the contents of this dissertation are original and have not been submitted in whole or in part for consideration for any other degree or qualification in this, or any other university. This dissertation is my own work and contains nothing which is the outcome of work done in collaboration with others, except as specified in the text and Acknowledgements. This dissertation contains fewer than 65,000 words including appendices, bibliography, footnotes, tables and equations and has fewer than 150 figures.

TUNEER CHAKRABORTY
JULY 2019

Acknowledgements

I'd like to acknowlwdge the mentorship and guidance provided by Shravan throughout my last two years as well as in this project. I also acknowledge the tireless work and unending enthusiasm of my collaborator, Srijan Bharati Das (Princeton) to bring this work to fruition. I also acknowledge many a fruitful discussions we've had with Samarth G K and Dr H M Antia, for getting handle on solar differential rotation.

Abstract

Yet to be written

Table of contents

Chapter 1

Introduction

1.1 What is global helioseismology?

Seismology is the study of vibration of material in a body on the surface to deduce its internal structure.

1.2 Frequency splittings in helioseismology

The standard solar model assumed in this work is that of a spherically symmetric, non-rotating, non-magnetic, adiabatic, isotropic, and static (SNRNMAIS). This SNRNMAIS model admits wave like solutions in density perubations (and as a result, displacement, pressure, etc also) [3]. Normal modes are found to have a discrete spectrum of eigen-frequencies to the operator

The essential idea which drives this work is that one can systematically deduce internal structure parameters, such as convective flow, differential rotation, magnetic fields etc by analysing the frequency splittings of solar acoustic resonant modes.

1.2.1 Quasi Degenerate Perturbation Theory

Quasi-degenerate pertubation theory requires us to account for mixing of modes which lie in a small neighbourhood on the frequency spectrum, and hence satisfy the quasi-degenerate condition.

$$|\omega_k^2 - \omega_{ref}^2| < \tau^2 \tag{1.1}$$

A general magnetohydrodynamic (MHD) description of the Sun using the MHD equations in its full vigour is rather cumbersome. Therefore, it is a standard practice ([8][7]) to implement the degenerate perturbation theory in finding the changes in eigenfrequencies from the standard solar model. This model assume the sun to be spherically symmetric, non-rotating, non-magnetic and non-attenuating. The equation of motion (in temporal fourier space) for such a model is given by [3]

$$\boldsymbol{\mathcal{L}}_0\boldsymbol{\xi} = \rho\omega^2\boldsymbol{\xi} = -\boldsymbol{\nabla}(\rho c^2\boldsymbol{\nabla}\cdot\boldsymbol{\xi} - \rho g\boldsymbol{\xi}\cdot\hat{\boldsymbol{e}}_r) - g\hat{\boldsymbol{e}}_r\boldsymbol{\nabla}\cdot(\rho\boldsymbol{\xi}) \tag{1.2}$$

where ω denotes the temporal frequency of oscillations, $c(r), g(r)$ and $\rho(r)$ are the radial functions of sounds speed, gravity and density. $\boldsymbol{\nabla}$ is the covariant spatial derivative operator. For all ensuing calculations and derivations we write equation 1.2 in the form $\boldsymbol{\mathcal{L}}_0\boldsymbol{\xi} = \rho\omega^2\boldsymbol{\xi}$ where the unperturbed wave operator $\boldsymbol{\mathcal{L}}_0$ is self-adjoint (CITE SOMETHING?). Axis-symmetric or non-axissymmetric flows, rotations, asphericities, anisotropies and non-radial variations in c, g, ρ can be captured as perturbation terms in equation 1.2. Although for the purpose of this study, we restrict ourselves to perturbations induced via presence of global scale magnetic fields only.

Because the solar eigenfunctions lack a toroidal component, we can denote the displacement field $\boldsymbol{\xi}(\boldsymbol{r},\omega)$ in the basis of spherical harmonics (and thereafter generalised spherical harmonics) as follows:

$$\boldsymbol{\xi}(\boldsymbol{r}) = \sum_k U_k(r)Y_l^m(\theta,\phi)\hat{\boldsymbol{e}}_r + V_k(r)\boldsymbol{\nabla}_1 Y_l^m(\theta,\phi) \tag{1.3}$$

$$= \sum_k \xi_k^0(r)Y_{lm}^0(\theta,\phi)\hat{\boldsymbol{e}}_0 + \xi_k^-(r)Y_{lm}^-(\theta,\phi)\hat{\boldsymbol{e}}_- + \xi_k^+(r)Y_{lm}^+(\theta,\phi)\hat{\boldsymbol{e}}_+ \tag{1.4}$$

Here, $\boldsymbol{r} = (r,\theta,\phi)$ in spherical polar coordinate system with basis vectors $(\hat{\boldsymbol{e}}_r, \hat{\boldsymbol{e}}_\theta, \hat{\boldsymbol{e}}_\phi)$, $\boldsymbol{\nabla}_1 \equiv= \left(\hat{\boldsymbol{e}}_\theta\partial_\theta + \hat{\boldsymbol{e}}_\phi\frac{1}{\sin\theta}\partial_\phi\right)$ and $k = (n,l,m)$ where n is the radial order, l is the angular degree and m is the azimuthal order of the particular SNRNMAIS mode. These basis vectors are related to those in generalised spherical harmonics' basis as:

$$\hat{\boldsymbol{e}}_- = \tfrac{1}{\sqrt{2}}(\hat{\boldsymbol{e}}_\theta - i\hat{\boldsymbol{e}}_\phi), \quad \hat{\boldsymbol{e}}_0 = \hat{\boldsymbol{e}}_r, \quad \hat{\boldsymbol{e}}_+ = -\tfrac{1}{\sqrt{2}}(\hat{\boldsymbol{e}}_\theta + i\hat{\boldsymbol{e}}_\phi) \tag{1.5}$$

We work with normalised eigenfunctions $\boldsymbol{\xi}_k$ with the spherically symmetric background density $\rho(r)$ as the weight factor, which satisfy the orthonormality condition:

$$(\boldsymbol{\xi}_{k'}|\rho\boldsymbol{\xi}_k) = \delta_{n'n}\delta_{l'l}\delta_{m'm} \tag{1.6}$$

where the inner product $(|)$ stands for $(\Phi|\Psi) \equiv \int_\odot d^3\mathbf{r}\Phi^*(\mathbf{r})\Psi(\mathbf{r})$.

1.3 Representation of Splitting Data

Since each multiplet ${}_nS_l$ contains $2l+1$ singlet modes, it is tedious to give the degree of splitting in the mode by exact value of each split frequency ω_{nlm} by itself. Therefore, in helioseismology, splitting data is represented by numbers called splitting coefficients which describe the decomposition of $\delta\omega_{nlm} = \omega_{nlm} - \omega_{nl}$ in terms of some basis function over m as follows

$$\omega_{nlm} = \omega_{nl} + \sum_{j=0}^{j_{max}} a_j^{nl}\mathcal{P}_j^{(l)}(m) \tag{1.7}$$

where $\mathcal{P}_j^{(l)}(m)$ with $j \in \{0, 1, 2, \ldots, j_{max}\}$ represents a $j_{max}+1$ dimensional orthogonal basis function of polynomials on the discrete space of m's which run from $-l$ to l. Since, there are $2l+1$ points in this discrete domain, the (vector) space spanned by all functions on this domain is $(2l+1)$ dimensional, which in turn means j_{max} cannot exceed $2l$. In practice, a-coefficients are recorded till a j_{max} of 10 ([9] for instace). We will use, as a standard, the basis functions prescribed in [8] which are Gram-Schmidt orthogonalised polynomials of increasing degree starting with $\mathcal{P}_0^{(l)}(m) = l$. Given the normalisation condition mentioned above, and this starting condition, the polynomials become well defined. A recipe for obtaining these can be found in Appendix A of [11]. Some properties to note about these polynomials are

- $\mathcal{P}_j^{(l)}(m)$ is odd/even about $m = 0$ if j is odd/even respectively.
- $\mathcal{P}_j^{(l)}(m)$ has polynomial degree j in m.
- $\mathcal{P}_j^{(l)}(m)$ contains only odd/even powers of m if j is odd/even respectively.
- In limit $l \gg 1$, $\mathcal{P}_j^{(l)}(m) \approx l P_j(m/l)$, where P_j is Legendre polynomial of degree j.

Once we have the splitting data ω_{nlm}, one can easily compute the a coefficients multiplying both sides of Eq.(1.7) by $\mathcal{P}_k^{(l)}(m)$,summing over all m, and finally using using the orthogonality condition

$$\sum_{m=-l}^{l} \mathcal{P}_j^{(l)}(m)\mathcal{P}_k^{(l)}(m) = \delta_{jk} \sum_{m=-l}^{l} \left(\mathcal{P}_j^{(l)}(m)\right)^2$$

as

$$a_j^{nl} = \sum_{m=-l}^{l} \delta\omega_{nlm}\mathcal{P}_j^{(l)}(m) \Big/ \sum_{m=-l}^{l} \left(\mathcal{P}_j^{(l)}(m)\right)^2 \tag{1.8}$$

Note that, even though scaled Legendre polynomials $lP_j(m/l)$ are not perfectly orthogonal on a discretised domain (under the inner product $(A|B) \sum_{m=-l}^{l} A^*(m)B(m)$), they are still linearly independent. However their use should be aovisded as a basis to represent splitting data because value of a-coefficients will change slightly depending on j_{max}, i.e. how many a coefficients are being fitted to the data; this occurs due to non-zero inner product between different basis functions. An orthogonal basis like $\mathcal{P}_j^{(l)}$ solves this issue by making a_j values independent of j_{max}.

Thus, henceforth whenever 'a-coefficients' are referred to in this text, it shall be understood that the underlying basis functions are given by $\{\mathcal{P}_j^{(l)} : j \in \{0, 1, \ldots, j_{max}\}\}$. The first few $\mathcal{P}^{(l)}$ are given below

$$\mathcal{P}_0^{(l)}(m) = l \tag{1.9}$$

$$\mathcal{P}_1^{(l)}(m) = m \tag{1.10}$$

$$\mathcal{P}_2^{(l)}(m) = \frac{3m^2 - l(l+1)}{2l-1} \tag{1.11}$$

Chapter 2

The Rotating Sun

2.1 Differential Rotation

The sun is known to rotate, unlike the earth, differentially. This means that angular rate of rotation of a point in the sun about its spin axis is depends on depth and latitude, $\Omega = \Omega(r, \theta)$. Splitting of p-mode frequencies due to differential rotationis well understood[8] and has a long history of inversion analysis[10]. This Ω is generally taken to be symmetric about the equitorial plane because the antisymmtric part of Ω is found to leave no signature in the acoustic frequency spcectrum in the first order as a result of a selection rule that arises from perturbation theory; this will be shown at the end of this chapter.

As a result of Alfven's freezing theorem, differential rotation is responsible for winding the solar magnetic field around its spin axis in an axis symmtric fashion. (refer something on this); thus for the most part we'll be investigating the effects of an axis symmetric magnetic field on the spectrum in this work.

2.2 Detection from frequency spectrum

Because of axis symmetry of differential rotation, the flow profile is given as,

$$\mathbf{v}_{rot} = \sum_{s=1,3,5,\ldots}^{\infty} -w_s^0(r)\partial_\theta Y_s^0 \hat{\boldsymbol{e}}_\phi \tag{2.1}$$

Note that w_1^0 is responsible for shell like (pure) rotation as it couples with $\partial_\theta Y_1^0 \propto \sin\theta$. Hence w_3^0 onwards components of flow are responsible for the differential part of the rotation. Finding frequency splittings due to differential rotatioin is a problem in degenrate perturbation (dpt) or quasi-degenerate perturbation theory depending on whether we're using the isolated multiplet assumption or not. Below we outline the qdpt approach to the problem because when applied to a single multiplet ${}_nS_l$ it reduces to the dpt approach; [7] contains a more detailed discussion on this topic; it, however, argues via analysis of ${}_nS_1$ and ${}_nS_3$ multiplets that eigenfrequency correction due to

mode-mixing between these two is negligible ($\sim 0.1\mu Hz$). I'll show in this work that for higher frequency modes with $l \sim 100$ a frequency correction close to $0.4\mu Hz$ is obtained when qdpt is used, which is close to the correction obtained due presence of realistically strong magnetic fields too, and hence cannot be ignored in an analysis which accounts for both differential rotation and magnetic fields.

2.2.1 QDPT Analysis

The pertubation operator $\delta\boldsymbol{\mathcal{L}}^{dr}$for a differential rotaional flow is given by

$$\delta\boldsymbol{\mathcal{L}}^{dr} = -2i\omega\rho\mathbf{v}_{rot}\cdot\boldsymbol{\nabla} \tag{2.2}$$

where ω is the reference frequency in the problem, and ρ is the static background density profile. The supermatrix element $Z_{k'k}$ for a pertubation $\delta\boldsymbol{\mathcal{L}}^{dr}$is given by

$$Z_{k'k} = \Lambda^{dr}_{k'k} - \delta_{k'k}(\omega^2_{ref} - \omega^2_k) \tag{2.3}$$

where Λ^{dr} is the coupling matrix element $\Lambda^{dr} = (\boldsymbol{\xi}_{k'}|\delta\boldsymbol{\mathcal{L}}^{dr}\boldsymbol{\xi}_k)$. Coupling matrix element is given by

$$\Lambda^{dr}_{k'k} = 8\pi\omega_{ref}\gamma_{l'}\gamma_l \sum_{s=1,3,5,\ldots} \gamma_s \begin{pmatrix} l' & s & l \\ -m & 0 & m \end{pmatrix} \int_\odot dr r^2 w^0_s(r) T_s(r) \tag{2.4}$$

where the sensitivity kernel T_s is given by

$$\begin{aligned} T_s(r) = (1-(-1)^{s+l+l'})\Omega^0_{l'}\Omega^0_l \begin{pmatrix} l' & s & l \\ -1 & 0 & 1 \end{pmatrix} r^{-1} \Big(U'V + V'U - U'U \\ - \frac{1}{2}\left(l'(l'+1) + l(l+1) - s(s+1)V'V\right)\Big) \end{aligned} \tag{2.5}$$

where the rounded brackets represent Wigner 3j symbols.

2.2.2 Selecition rules in mode coupling

This matrix element enforces the following selection rules for inter-mode interaction which derive from the properties of Wigner 3j symbols [7].

1. $m' = m$
2. $l' + l + s = \text{odd}$
3. $|l' - l| \leq s \leq l' + l$

It should be noted here that even though only sum over odd s is considered, the expression for T_s is general and holds for all s. This has been verified independently using the Mathematica packaged developed for the sake of this work. This means as far as self coupling is concerned ($l' = l$), the matrix element vanish for all even s.

Form of supermatrix $Z_{k'k}$

It is clear from selection rule (1) in 2.2.2 that $Z_{k'k}$ is going to be a sparse matrix consisting of a diagonal and a number of sub-diagonals (proportional to number of multiplets being considered). Also, as s is always odd, $l - l'$ has to be even for non-zero coupling as consequence of selection rule (2). This influences our choice of modes whose inter-coupling will be studied hereafter. Figure (2.1) is a visual representation of a typical supermatrix consisting of three multiplets.

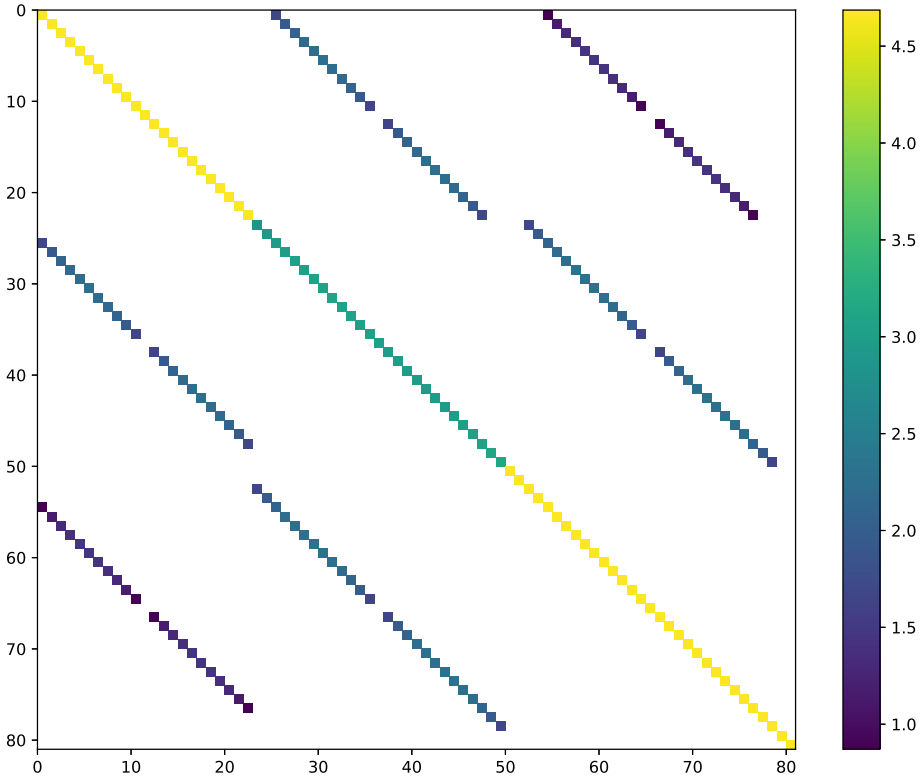

Fig. 2.1 Visualisation of $\log_{10}|Z_{k'k}|$ in μHz^2 for the modes ${}_0S_{11}$, ${}_0S_{13}$, and ${}_0S_{15}$ with frequencies $603.69\mu Hz$, $641.84\mu Hz$, and $677.55\mu Hz$ respectively. White spaces correspond to 0 value. Logarithm scale demonstrates the order of magnitude difference between self-coupling (diagonal elements), and cross-coupling (subdiagonal elements).Also notice that largest elements (yellow) are in the first and third section in the main diagonal. These are large because these frequencies are placed away from ω_{ref} which is taken to be mean of the three mode frequencies. The relative weakness of the sub-diagonal terms compared to the main-diagonals is because $l - l' \geq 2$ forces $s \geq 2$ which makes the largest component of differential rotation, i.e. w_1^0, unable to couple these modes; w_3^0 and w_5^0 are one and two orders of magnitude smaller than w_1^0 respectively.

Chapter 3

Internal Magnetic Fields

3.1 Solar Magnetic Field

It is well known through the observation of much surface solar phenomenon like active regions, solar flares, coronal mass ejections etc, that the sun has in its interior, often highly localised, significant magnetic fields. The source of this magetic field is theorised to be a primordial current which started a dynamo process that is kept going at the expense of continous dissipation of energy from the solar bulk (CITE DYNAMO). It is also widely belived however that mean magnetic field throughout the solar bulk is fairly weak. This chapter is devoted to finding a method to observe signature of this magnetic field in the p-mode frequency spectrum.

Most of high intensity magnetic activity is limited to the solar surface. The tachocline is believed to contain toroidal fields as high as 10^5G (CITE TACH). outside the tachocline the magnetic field is believed to be mostly dipolar such that mean surface magnetic field is about 10G. Very strong local magnetic fields apart from these are also known to exist, but detection of such fields is outside the scope of this work; here we shall only investigate the effect of *global* fields. It will be shown in this chapter why the method of frequency splittings is not the best way to detect strongly localised magentic fields.

3.2 Equation of Motion

In the presence of background magnetic field $\mathbf{B}$, the equation of motion is governed by the new operator $\boldsymbol{\mathcal{L}} \to \boldsymbol{\mathcal{L}} + \delta\boldsymbol{\mathcal{L}}^B$, where $\delta\boldsymbol{\mathcal{L}}^B$ is estabished in [6] as below.

$$\begin{aligned}\delta\boldsymbol{\mathcal{L}}^B\boldsymbol{\xi} = \frac{-1}{4\pi}\boldsymbol{\nabla}\cdot[&\mathbf{BB}\cdot\boldsymbol{\nabla\xi} + \mathbf{B}\cdot\boldsymbol{\nabla\xi}\mathbf{B} - 2\mathbf{BB}\boldsymbol{\nabla}\cdot\boldsymbol{\xi} - (\boldsymbol{\xi}\cdot\boldsymbol{\nabla}\mathbf{B})\mathbf{B} - \mathbf{B}(\boldsymbol{\xi}\cdot\boldsymbol{\nabla}\mathbf{B}) \\ &+ B^2\boldsymbol{\nabla}\cdot\boldsymbol{\xi}\boldsymbol{I} - \mathbf{BB}:\boldsymbol{\nabla\xi}\boldsymbol{I} + \boldsymbol{\xi}\cdot\boldsymbol{\nabla}\frac{B^2}{2}\boldsymbol{I}]\end{aligned} \tag{3.1}$$

where the : stands for contraction of two second rank tensors ($\mathbf{P}:\mathbf{Q} \equiv P_{ij}Q_{ji}$).

Note that in above expression $\mathbf{B}$ only appears in the second order. This is a consequence of the induction equation where the Lagrangian displacement field $\boldsymbol{\xi}$ creates a current $\mathbf{j} \propto \boldsymbol{\xi} \times \mathbf{B}$ and this current interacts with magnetic field as $\mathbf{j} \times \mathbf{B}$ to give rise to acceleration. [5] contains a detailed derivation of this and a proof of self adjointedness for $\delta\boldsymbol{\mathcal{L}}^B$.

This expression can be put in a more convenient form involving the Lorentz stress tensor $\boldsymbol{\mathcal{H}} \equiv \mathbf{BB}$ as

$$\delta\boldsymbol{\mathcal{L}}^B\boldsymbol{\xi} = \frac{-1}{4\pi}\boldsymbol{\nabla}\cdot[\boldsymbol{\mathcal{H}}\cdot\boldsymbol{\nabla}\boldsymbol{\xi}+(\boldsymbol{\nabla}\boldsymbol{\xi})^T\cdot\boldsymbol{\mathcal{H}}-2\boldsymbol{\mathcal{H}}\boldsymbol{\nabla}\cdot\boldsymbol{\xi}-\boldsymbol{\xi}\cdot\boldsymbol{\nabla}\boldsymbol{\mathcal{H}}+\boldsymbol{\mathcal{H}}:\boldsymbol{I}\boldsymbol{\nabla}\cdot\boldsymbol{\xi}\boldsymbol{I}-\boldsymbol{\mathcal{H}}:\boldsymbol{\nabla}\boldsymbol{\xi}\boldsymbol{I}+\boldsymbol{\xi}\cdot\boldsymbol{\nabla}\left(\frac{\boldsymbol{\mathcal{H}}:\boldsymbol{I}}{2}\right)\boldsymbol{I}] \tag{3.2}$$

The tensor $\boldsymbol{\mathcal{H}}$ is the quantity of interest in this problem and any inversion algorithm must first invert splitting data for its components. It remains unclear if the magnetic field can be recovered from just the knowldge of components of $\boldsymbol{\mathcal{H}}$.

3.3 Coupling Matrix

3.3.1 Lorentz Stress components

The process of taking integrals over a sphere becomes simplified if we're operating in the Generalised Sopherical Harmonics formalism. In this formalism (look at A for basis of this formalism), magnetic field and Lorentz stress are decomposed as

$$\mathbf{B} = \sum_{st}\sum_{\alpha} B^{\alpha}_{st}(r)Y^{\alpha}_{st}(\theta,\phi)\hat{\boldsymbol{e}}_{\alpha}$$

$$\boldsymbol{\mathcal{H}} = \sum_{st}\sum_{\mu\nu} h^{\mu\nu}_{st}(r)Y^{\mu+\nu}_{st}(\theta,\phi)\hat{\boldsymbol{e}}_{\mu}\hat{\boldsymbol{e}}_{\nu}$$

where the generalised spherical harmonic (GSH) coordinate indices given by Greek symbols run from -1 to $+1$. It is not very productive to find general expressions relating $\mathbf{B}$ components to $\boldsymbol{\mathcal{H}}$ components. Instead, we'll find special relations pertaining to the kind of magnetic field at hand when necessary. $\boldsymbol{\mathcal{H}}$ by construction satisfies the symmetry property $h^{\mu\nu}_{st} = h^{\nu\mu}_{st}$ ($\because \boldsymbol{\mathcal{H}} = \mathbf{BB}$), and $(h^{\mu\nu}_{st})^* = (-1)^t h^{\bar{\mu}\bar{\nu}}_{s\bar{t}}$, where overbars represent negatives, follows from its realness condition.

3.3.2 Sensitivity Kernels

Coupling matrix element is given as on integral transform over $\boldsymbol{\mathcal{H}}$ as

$$\Lambda^B_{k'k} = (\boldsymbol{\xi}_{k'}|\delta\boldsymbol{\mathcal{L}}^B\boldsymbol{\xi}_k) = \int_0^{R_\odot} drr^2 \sum_{\substack{st\\ \mu\nu}} \mathcal{B}^{\mu\nu}_{st}(r)h^{\mu\nu}_{st}(r) \tag{3.3}$$

where $\mathcal{B}^{\mu\nu}_{st}$ are the eigenfunction dependent magnetic sensitivity kernels. Prescription for evaluating these kernels and the explicit expressions can be found in [6]. It should

be noted however that the coupling integral $(\boldsymbol{\xi}_{k'}|\delta\boldsymbol{\mathcal{L}}^B\boldsymbol{\xi}_k)$ can be reduced to the radial integral form obtained in (3.3) contains no boundary terms. It is indeed the case that the magnetic field is assumed to vanish at the surface in this analysis. Relaxing this assumption will introduce boundary terms which involve integrals only over the solar surface. Since $h^{\mu\nu}_{st}$ is symmetric in interchange of μ and ν, we may ascribe the same symmetry to $\mathcal{B}^{\mu\nu}_{st}$ too without any loss in generality.

Using the Mathematica package developed for this work [2] which automates manipulation of tensor spherical harmonics via the method of GSHs, the following forms of the kernels were found

$$\begin{aligned}\mathcal{B}^{--}_{st} = \frac{(-1)^{m'+1}}{r^2}\gamma_l\gamma_{l'}\gamma_s\begin{pmatrix} l' & s & l \\ -m' & t & m\end{pmatrix}\Big\{&\begin{pmatrix} l' & s & l \\ 1 & -2 & 1\end{pmatrix}\Omega^0_l\Omega^0_{l'}\left[\left(U+\Omega^{2\,2}_{l'}V\right)V' - UU' - rV\dot{V}'\right]\\ &+\begin{pmatrix} l' & s & l \\ 2 & -2 & 0\end{pmatrix}\Omega^0_{l'}\Omega^2_{l'}\left[(U+r\dot{U})V' - rU\dot{V}'\right] + \begin{pmatrix} l' & s & l \\ 0 & -2 & 2\end{pmatrix}\Omega^0_l\Omega^2_l rV\dot{U}'\\ &+\begin{pmatrix} l' & s & l \\ 3 & -2 & -1\end{pmatrix}\Omega^0_l\Omega^0_{l'}\Omega^2_{l'}\Omega^3_{l'}VV'\Big\}\end{aligned} \tag{3.4}$$

$$\begin{aligned}2\mathcal{B}^{0-}_{st} = \frac{(-1)^{m'}}{r^2}\gamma_l\gamma_{l'}\gamma_s\begin{pmatrix} l' & s & l \\ -m' & t & m\end{pmatrix}\Big\{&\begin{pmatrix} l' & s & l \\ 0 & -1 & 1\end{pmatrix}\Omega^0_l\Big[\left(2U+\Omega^{2\,2}_{l'}V\right)U'\\ &+\Omega^{0\,2}_{l'}\left(-2UV' - VV' + rV\dot{V}'\right) - r\left(U+V-r\dot{V}'\right)\dot{U}'\Big]\\ &-\begin{pmatrix} l' & s & l \\ 1 & -1 & 0\end{pmatrix}\Omega^0_{l'}\left[(-2U+\Omega^{0\,2}_l V)U' + \Omega^{0\,2}_l V\left(r\dot{V}' - V'\right)\right.\\ &\left.+U\left(2V' + r(\dot{U}' - 2\dot{V}' + r\ddot{V}')\right)\right] + \begin{pmatrix} l' & s & l \\ -1 & -1 & 2\end{pmatrix}\Omega^0_l\Omega^0_{l'}\Omega^2_l V\left[U' - V' + r\dot{V}'\right]\\ &+\begin{pmatrix} l' & s & l \\ 2 & -1 & -1\end{pmatrix}\Omega^0_l\Omega^0_{l'}\Omega^2_{l'}\left[V\left(U' - 3V' + r\dot{V}'\right) + 2r\dot{V}V'\right]\Big\}\end{aligned} \tag{3.5}$$

$$\begin{aligned}\mathcal{B}^{00}_{st} = \frac{(-1)^{m'}}{2r^2}\gamma_l\gamma_{l'}\gamma_s\begin{pmatrix} l' & s & l \\ -m' & t & m\end{pmatrix}(1+p)\Big\{&\frac{1}{2}\begin{pmatrix} l' & s & l \\ 0 & 0 & 0\end{pmatrix}\left[\left(6U - 4\Omega^{0\,2}_l V - 2r\dot{U}\right)\left(U' - \Omega^{0\,2}_{l'}V'\right)\right.\\ &\left.+2\Omega^{0\,2}_{l'}rU\dot{V}' + r\left(\left(-4U + 2\Omega^{0\,2}_l V + r\dot{U}\right)\right)\dot{U}' + rU\ddot{U}'\right]\\ &-\begin{pmatrix} l' & s & l \\ -1 & 0 & 1\end{pmatrix}\Omega^0_{l'}\Omega^0_l\left[V\left(-4U' + 2\left(1+\Omega^{0\,2}_{l'}\right)V' + r\left(\dot{U}' - 2\dot{V}'\right)\right) + 2r\dot{V}\left(U' - V' + r\dot{V}'\right)\right]\Big\}\end{aligned} \tag{3.6}$$

$$\begin{aligned}2\mathcal{B}^{+-}_{st} = \frac{(-1)^{m'}}{r^2}\gamma_l\gamma_{l'}\gamma_s\begin{pmatrix} l' & s & l \\ -m' & t & m\end{pmatrix}(1+p)\Big\{&-2\begin{pmatrix} l' & s & l \\ -2 & 0 & 2\end{pmatrix}\Omega^0_l\Omega^2_l\Omega^0_{l'}\Omega^2_{l'}VV'\\ &+\begin{pmatrix} l' & s & l \\ -1 & 0 & 1\end{pmatrix}\Omega^0_{l'}\Omega^0_l\left[-rV\dot{U}' + U\left(U' - V' + r\dot{V}'\right)\right] + \begin{pmatrix} l' & s & l \\ 0 & 0 & 0\end{pmatrix}r^2\left[U\ddot{U}' - \dot{U}\dot{U}'\right]\Big\}\end{aligned} \tag{3.7}$$

where $p \equiv (-1)^{l'+l+s}$, $U, V \equiv U_{nl}, V_{nl}$, and $U', V' \equiv U_{n'l'}, V_{n'l'}$.

Kernel components $\mathcal{B}^{\mu\nu}_{st}$ are found to have these following properties:

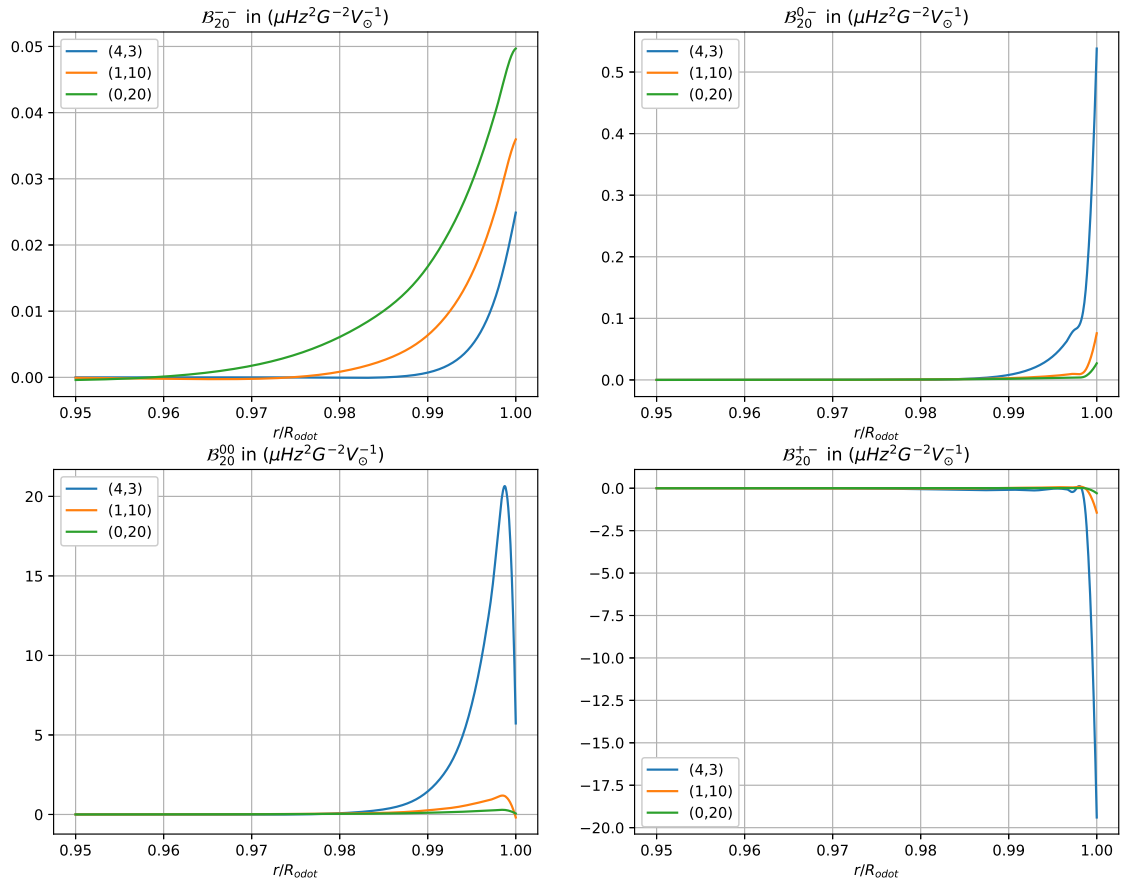

Fig. 3.1 Self coupling Kernels for the modes ${}_4S_3$, ${}_1S_{10}$, and ${}_0S_{20}$.

1. $\mathcal{B}_{st}^{\mu\nu} = \mathcal{B}_{st}^{\nu\mu}$ (by construction)
2. $\mathcal{B}_{st}^{--} = (-1)^{l+l'+s}\mathcal{B}_{st}^{++}$
3. $\mathcal{B}_{st}^{0-} = (-1)^{l+l'+s}\mathcal{B}_{st}^{+0}$
4. $\mathcal{B}_{st}^{00} = \mathcal{B}_{st}^{+-} = \mathcal{B}_{st}^{-+} = 0$ for odd $(l' + l + s)$

Figure (3.1) shows the four independent components of the sensitivity kernel under self coupling for some modes. It is clear from the plots that for all modes, sensitivity is mostly localised to the solar boundary. This effect is most striking for $\mathcal{B}_{st}^{+-}$ across modes. This is a an indirect consequence of the background density profile of the sun which falls almost exponentially fast with respect to radius towards the outer regions of the sun. The low density near the boundary makes the eigenfunction peak distinctly near the boundary. However, as can be seen in equations (3.4), (3.5), (3.6), and (3.7),

the kernels depend quadratically on U and V, which finally makes them peak at the boundary. This implies that most of the magnetic splitting caused is due to the fields near the surface and acts as limitation to imaging the interior magnetic precisely via an inversion of frequency splitting data.

3.4 Synthetic Magnetic Field

Using some basic pieces of information about mean solar magnetic field as given in 3.1, we can posit the following form of a synthetic magnetic field which will be used for validating our routine of finding frequency splits. We give the following form of the magnetic field which is comoposed of an internal toroidal field concentrated at the tachocline, and a dipolar field which extends from the tachocline to the surface.

3.4.1 Construction of B

Using the identities $\boldsymbol{\nabla}_1 Y_l^m = \Omega_l^0 \left(Y_{lm}^{-1}\hat{\boldsymbol{e}}_- + Y_{lm}^0\hat{\boldsymbol{e}}_+\right)$, $\hat{\boldsymbol{e}}_r \times \boldsymbol{\nabla}_1 Y_l^m = i\Omega_l^0 \left(Y_{lm}^{-1}\hat{\boldsymbol{e}}_- - Y_{lm}^0\hat{\boldsymbol{e}}_+\right)$, and $Y_1^0(\theta,\phi) = \gamma_1 \cos\theta$ we see following things: (1) A toroidal field $\mathbf{B} = \alpha(r)\sin\theta\hat{\boldsymbol{e}}_\phi$ can be given as $B_{10} = i\alpha(r)/\gamma_1\,(-1,0,1)$ with all other B_{st} components being 0, and (2) A dipolar field $\mathbf{B} = \beta(r)(2\cos\theta\hat{\boldsymbol{e}}_r + \sin\theta\hat{\boldsymbol{e}}_\theta)$ with $\beta \propto r^{-3}$ can be given as $B_{10} = -\beta(r)/\gamma_1\,(1,-2,1)$ with all other B_{st} components being 0. Note that the row vector refers to the GSH coordinate index μ. This leads to the following final form of $\mathbf{B}$

$$B_{st}(r) = \begin{cases} -i\frac{\alpha(r)}{\gamma_1}\begin{pmatrix}1\\0\\-1\end{pmatrix} - \frac{\beta(r)}{\gamma_1}\begin{pmatrix}b - r\dot{b}\\-2b\\b - r\dot{b}\end{pmatrix}, & \text{for}(s,t) = (1,0) \\ 0, & \text{for}(s,t) \neq (1,0) \end{cases} \tag{3.8}$$

where $b(r) = 1$ where field is perfectly dipolar. The term $r\dot{b}(r)$ appear as a consequence of fixing the diveregence to zero and is only nonzero in the transition region where $b(r)$ goes from 0 to 1. It was can be checked via using $\boldsymbol{\nabla}\cdot\mathbf{B} = g_{\alpha\beta}(\boldsymbol{\nabla}\mathbf{B})^{\alpha\beta}$ ([2] was used) that the two parts in (3.8) (toroidal and dipolar) satisfy the solenoidal condition independently. We plot the forms of the α, β, and b used in our frequency splitting calculations.

3.4.2 Construction of $\mathcal{H}$

After the form of $\mathbf{B}$ has been ascertained, it is straighforward to derive components of $\boldsymbol{\mathcal{H}}$ via taking a tensor product. Decomposing either field in their GSH forms as in 3.3.1, and using orthonormality relation

$$\int d\Omega \left(Y_{l_1m_1}^{n_1}\right)^* Y_{l_2m_2}^{n_2} = \delta_{l_1l_2}\delta_{m_1m_2}\delta_{N_1N_2} \tag{3.9}$$

and the triple integral result

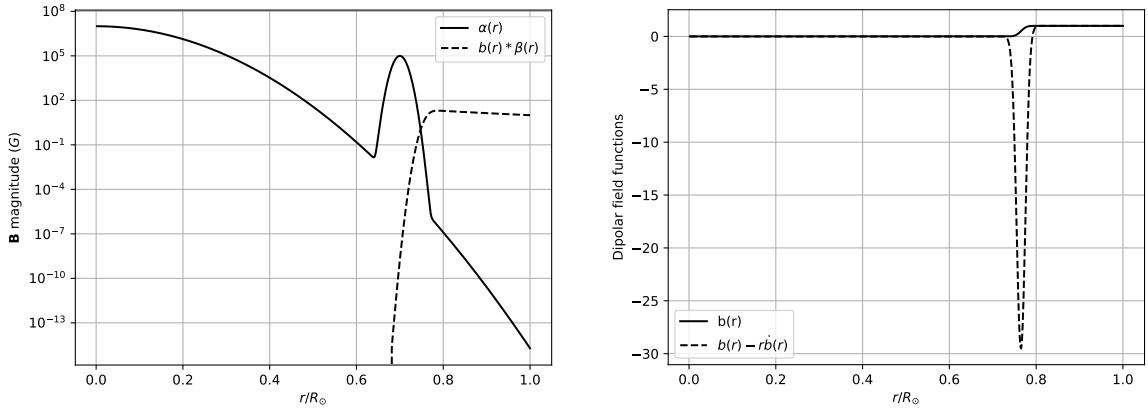

(a) α and $b * \beta$ in G

(b) b and $a = b - r\dot{b}$

Fig. 3.2 $\alpha(r)$ is addition of two Gaussians centred at $r = 0$ with peak $10^7 G$ and at $r = 0.7R_\odot$ with peak $10^5 G$ respectively. b transitions smoothly from 0 to 1 as a sigmoid around $r = 0.7R_\odot$. $r = 0.7R_\odot$ mark is roughly where the tachocline is placed. Figure (3.2a) shows the poloidal (dipolar) field β starting to dominate over the toroidal field by atleast three orders of magnitude as r exceeds $\sim 0.8R_\odot$.

$$\int d\Omega \left(Y^{N_1}_{l_1 m_1}\right)^* Y^{N_2}_{l_2 m_2} Y^{N_3}_{l_3 m_3} = (-1)^{m_1+N_1} 4\pi \gamma_{l_1}\gamma_{l_2}\gamma_{l_3} \begin{pmatrix} l_1 & l_2 & l_3 \\ -m_1 & m_2 & m_3 \end{pmatrix} \begin{pmatrix} l_1 & l_2 & l_3 \\ -N_1 & N_2 & N_3 \end{pmatrix} \tag{3.10}$$

one can write

$$h^{\mu\nu}_{st} = \sum_{\substack{s_1 t_1 \\ s_2 t_2}} \langle Y^{\mu+\nu}_{st}, Y^{\mu}_{s_1 t_1} Y^{\nu}_{s_2 t_2} \rangle B^{\mu}_{s_1 t_1} B^{\nu}_{s_2 t_2} \tag{3.11}$$

Where $\langle Y^{n_1}_{l_1 m_1}, Y^{N_2}_{l_2 m_2} Y^{N_3}_{l_3 m_3} \rangle$ stands for the integral in eq(3.10). If $\mathbf{B}$ has only $s = s_0$ and $t = t_0$ features, that is $\mathbf{B} = \sum_\alpha B^\alpha_{s_0 t_0} Y^\alpha_{s_0 t_0} \hat{\boldsymbol{e}}_\alpha$, components of $\boldsymbol{\mathcal{H}}$ are given by

$$h^{\mu\nu}_{st} = B^{\mu}_{s_0 t_0} B^{\nu}_{s_0 t_0} (-1)^{\mu+\nu+t} (2s_0 + 1) \gamma_s \begin{pmatrix} s_0 & s & s_0 \\ \mu & -(\mu+\nu) & \nu \end{pmatrix} \begin{pmatrix} s_0 & s & s_0 \\ t_0 & -t & t_0 \end{pmatrix} \tag{3.12}$$

For the axis symmetric magnetic field constructed in 3.4.1, we may set $s_0 = 1$ and $t_0 = 0$. Wigner 3j selection rules given in 2.2.2 dicate that $\boldsymbol{\mathcal{H}}$ can only have $s = 0, 1, 2$ and $t = 0$. Then we have the form

$$h^{\mu\nu}_{s0} = 3\gamma_s B^{\mu}_{10} B^{\nu}_{10} (-1)^{\mu+\nu} \begin{pmatrix} 1 & s & 1 \\ \mu & -(\mu+\nu) & \nu \end{pmatrix} \begin{pmatrix} 1 & s & 1 \\ 0 & 0 & 0 \end{pmatrix} \tag{3.13}$$

But we know that $\begin{pmatrix} 1 & s & 1 \\ 0 & 0 & 0 \end{pmatrix}$ vanishes for odd s. Thus we note here that $\boldsymbol{\mathcal{H}}$ has no $s = 1$ and has non-zero $s = 0$ components, which is different from how differential rotation couples modes. The $s = 0$ feature of the Lorentz stress tensor indicates a net shift from

the unperturbed mode frequency ω_{nl} for a particular multiplet ${}_nS_l$ as this term couples with $\begin{pmatrix} l' & 0 & l \\ -m & 0 & m \end{pmatrix}$ which is independent of m.

Chapter 4

Results

4.1 Frequency Splittings due to Differential Rotation

In this treatment we show that while taking very closely spaced multiplets, the isolated multiplet condition breaks down and there is significant cross coupling across modes due to differential rotation alone. Because axis symmetry imposes the $m' = m$ selection rule, the supermatrix $Z_{k'k}$ of perturbation $\delta\boldsymbol{\mathcal{L}}^{dr}$ is a sparse matrix consisting of diagonals and subdiagonal as show in figure (2.1). As a case study, we choose to investigate the splitting coefficients of the mode ${}_0S_{77}$ as a result of cross coupling with its neighbouring modes which all lie withing an interval of $100\mu Hz$.

4.1.1 Splitting with pure rotation

We plot the split frequencies ${}_0S_{77}$ along with some neighbouring modes to contrast the results obtained from a dpt and a qdpt analysis.

A coefficients obtained from the split is tabulated

4.1.2 Splitting with pure rotation removed

After removing a constant 440nHz from the w_1^0/r rotational profile, we get the following splitting of frequencies for dpt and qdpt respectively as shown in 4.1. Qdpt is performed taking 5 modes all lying in a band of width $100\mu Hz$.

4.64e-310	4.64e-310	6.91e-310
6.91e-310	4.75e-309	1.64e-287

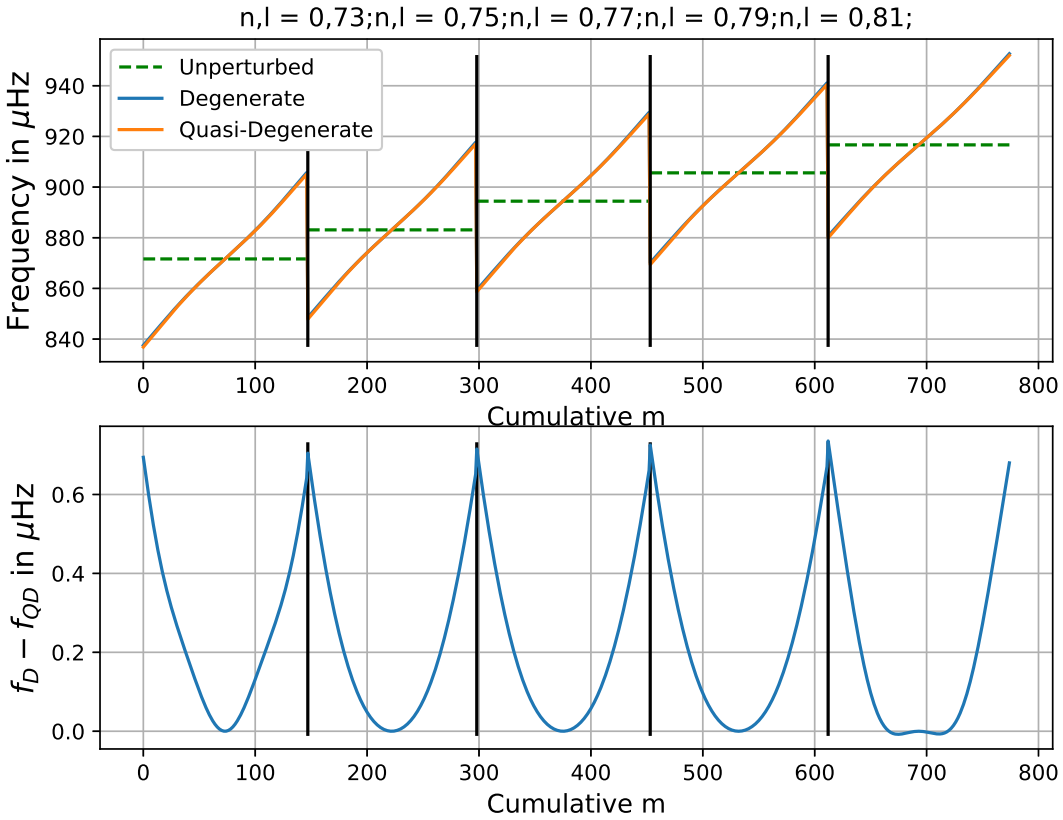

Fig. 4.1 Dpt and Qdpt splits with ${}_0S_{73}$, ${}_0S_{75}$, ${}_0S_{77}$, ${}_0S_{79}$, and ${}_0S_{81}$ which have frequencies $871.63\mu Hz$, $883.12\mu Hz$, $894.43\mu Hz$, $905.62\mu Hz$, and $916.66\mu Hz$ respectively. Top plot shows frequency splittings of the five modes and their unperturbed frequencies. Bottom plot shows the departure of the qdpt frequencies from the dpt frequencies.

4.1.3 QDPT vs DPT with increasing coupling modes

4.2 Splittings due to Lorentz Stresses

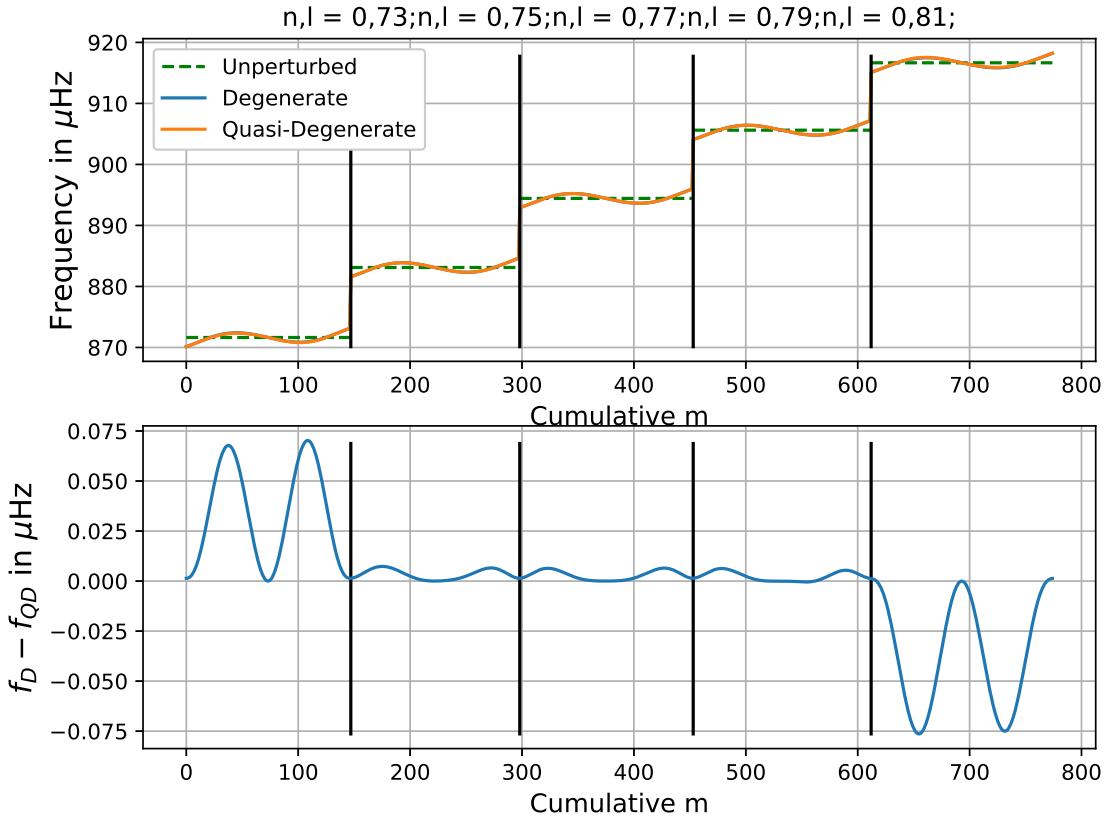

Fig. 4.2 Dpt and Qdpt splits with $440nHz$ removed from w_1^0 for modes ${}_0S_{73}$, ${}_0S_{75}$, ${}_0S_{77}$, ${}_0S_{79}$, and ${}_0S_{81}$ which have frequencies $871.63\mu Hz$, $883.12\mu Hz$, $894.43\mu Hz$, $905.62\mu Hz$, and $916.66\mu Hz$ respectively. Top plot shows frequency splittings of the five modes and their unperturbed frequencies. Bottom plot shows the departure of the qdpt frequencies from the dpt frequencies.

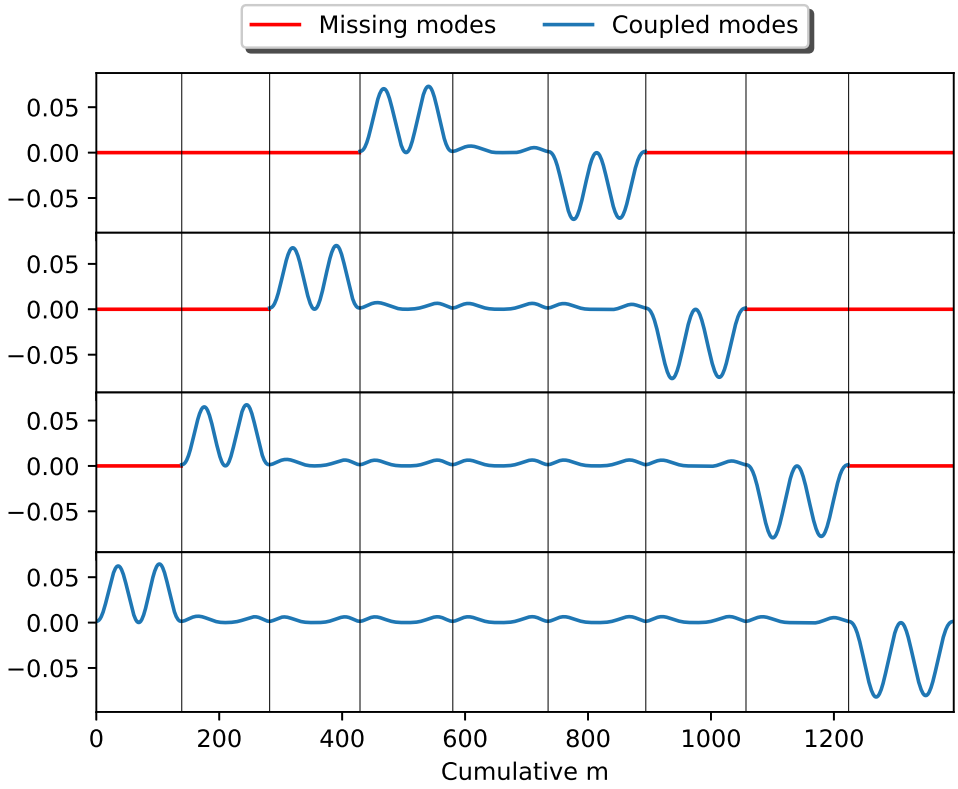

Fig. 4.3 Shows the difference between frequencies obtained from qdpt and dpt when different number of neighbouring modes are allowed to couple. From top it shows ${}_0S_{77}$ coupling with two, four, six, and eight closest $\Delta l = 2$ neighbours as listed in table

References

[1] Chakraborty, T. and Das, S. B. (2019a). Main repository for lorentz stress splitting calculation. https://github.com/tuneerch/lorentz_stress_kernel. Accessed: 2019-07-18.

[2] Chakraborty, T. and Das, S. B. (2019b). Mathematica package for generalised spherical harmonic manipulation. https://github.com/tuneerch/LStress_Mathematica. Accessed: 2019-07-17.

[3] Christensen–Dalsgaard, J. (2003). *Lecture Notes on Stellar Oscillations*. Fifth edition.

[4] Dahlen, F. A. and Tromp, J. (1998). *Theoretical Global Seismology*. Princeton University Press.

[5] Goedbloed, J. P. H. and Poedts, S. (2004). *Principles of Magnetohydrodynamics: with Applications to Laboratory and Astrophysical Plasmas*. Cambridge University Press.

[6] Hanasoge, S. M. (2017). Seismic sensitivity of normal-mode coupling to Lorentz stresses in the Sun. *Monthly Notices of the Royal Astronomical Society*, 470:2780–2790.

[7] Lavely, E. M. and Ritzwoller, M. H. (1992). The Effect of Global-Scale, Steady-State Convection and Elastic-Gravitational Asphericities on Helioseismic Oscillations. *Philosophical Transactions of the Royal Society of London Series A*, 339:431–496.

[8] Ritzwoller, M. H. and Lavely, E. M. (1991). A unified approach to the helioseismic forward and inverse problems of differential rotation. *The Astrophysical Journal*, 369:557–566.

[9] Schou, J. (1999). Index of / schou/anavw72z. http://quake.stanford.edu/~schou/anavw72z/?C=M;O=A. Accessed: 2019-07-17.

[10] Schou, J., Antia, H. M., Basu, S., Bogart, R. S., Bush, R. I., Chitre, S. M., Christensen-Dalsgaard, J., di Mauro, M. P., Dziembowski, W. A., Eff-Darwich, A., Gough, D. O., Haber, D. A., Hoeksema, J. T., Howe, R., Korzennik, S. G., Kosovichev, A. G., Larsen, R. M., Pijpers, F. P., Scherrer, P. H., Sekii, T., Tarbell, T. D., Title, A. M., Thompson, M. J., and Toomre, J. (1998). Helioseismic Studies of Differential Rotation in the Solar Envelope by the Solar Oscillations Investigation Using the Michelson Doppler Imager. *The Astrophysical Journal*, 505:390–417.

[11] Schou, J., Christensen-Dalsgaard, J., and Thompson, M. (1994). On comparing helioseismic two-dimensional inversion methods. *The Astrophysical Journal*, 433.

Appendix A

Generalised Spherical Harmonics Formalism

A.1 Formalism

A general Formalism to describe complex tensor fields on the surface of a 2-sphere is that of Generalised Spherical Harmonics. (CREATORS) propose a generalisation of the spherical harmonic given by Y_{lm}^N, with an added index N, it reduces to the spherical harmonics when $N = 0$.

$$Y_{lm}^0(\theta, \phi) = Y_l^m(\theta, \phi) \tag{A.1}$$

These functions couple with the GSH unit vectors given by

$$\hat{\boldsymbol{e}}_- = \tfrac{1}{\sqrt{2}}(\hat{\boldsymbol{e}}_\theta - i\hat{\boldsymbol{e}}_\phi), \quad \hat{\boldsymbol{e}}_0 = \hat{\boldsymbol{e}}_r, \quad \hat{\boldsymbol{e}}_+ = -\tfrac{1}{\sqrt{2}}(\hat{\boldsymbol{e}}_\theta + i\hat{\boldsymbol{e}}_\phi) \tag{A.2}$$

to form tensor spherical harmonics

$$\mathbf{Y}_{lm}^N \equiv Y_{lm}^N \hat{\boldsymbol{e}}_{\alpha_1} \hat{\boldsymbol{e}}_{\alpha_2} \dots \hat{\boldsymbol{e}}_{\alpha_q} \tag{A.3}$$

where $\alpha_1 + \alpha_2 + \ldots + \alpha_q = N$. These tensor functions by construction are eigenfunctions of the total angular momentum operator $\hat{\mathbf{J}} = \hat{\mathbf{L}} + \hat{\mathbf{s}}$, where the first part $\hat{\mathbf{L}}$ is the rotational generator for the scalar part of a field and the latter part $\hat{\mathbf{s}}$ generates rotation of the vector basis. Explicit expressions for Y_{lm}^N can be found in [4]. Eigenvalues are as below

$$\hat{J}_z \mathbf{Y}_{lm}^N = m\mathbf{Y}_{lm}^N \tag{A.4}$$

$$\hat{J}^2 \mathbf{Y}_{lm}^N = l(l+1)\mathbf{Y}_{lm}^N \tag{A.5}$$

A.2 Conventions

$$\gamma_l \equiv \frac{2l+1}{4\pi} \tag{A.6}$$

$$\Omega_l^N \equiv \sqrt{\frac{(l+N)(l-N+1)}{2}} \tag{A.7}$$

Note that $\Omega_l^{-N} = \Omega_l^{N+1}$.

$$g_{\mu\nu} \equiv \hat{\boldsymbol{e}}_\mu \cdot \hat{\boldsymbol{e}}_\nu = \begin{pmatrix} 0 & 0 & -1 \\ 0 & 1 & 0 \\ -1 & 0 & 0 \end{pmatrix} \tag{A.8}$$

$$\hat{\boldsymbol{e}}_\mu^* \cdot \hat{\boldsymbol{e}}_\nu = \delta_{\mu\nu} \tag{A.9}$$

A.3 Integrals

$$\int_0^{2\pi} d\phi \int_0^{\pi} d\theta \sin\theta Y_{l_1 m_1}^{N_1} Y_{l_2 m_2}^{N_2} Y_{l_3 m_3}^{N_3} = 4\pi \gamma_{l_1}\gamma_{l_2}\gamma_{l_3} \begin{pmatrix} l_1 & l_2 & l_3 \\ N_1 & N_2 & N_3 \end{pmatrix} \begin{pmatrix} l_1 & l_2 & l_3 \\ m_1 & m_2 & m_3 \end{pmatrix} \tag{A.10}$$

Explicit expressions for $\begin{pmatrix} l_1 & l_2 & l_3 \\ m_1 & m_2 & m_3 \end{pmatrix}$ can be found in [4]. The property $\left(Y_{lm}^N\right)^* = (-1)^{m+N} Y_{l\bar{m}}^{\bar{N}}$ makes it useful while taking inner products of tensor fields in our analysis. Note that works like [7], [6] etc. use a slighlty different convention defining Y_{lm}^N as Y_{lm}^N/γ_l as in our convention. In this work, we have followed the convention of [4].

A.4 Rotation

Tensor GSH functions $\mathbf{Y}_{lm}^N$ obey the same rotation laws as spherical harmonics Y_l^m. Given two coordinate systems (θ, ϕ) and (θ', ϕ') such that $\phi = 0$ and $\phi' = 0$ planes coincide and on that plane $\theta' = \theta - \beta$, which corresponds to the primed axis being tilted by an angle β to the unprimed axis, the GSH functions in the new coordinate system is given by

$$\mathbf{Y}_{lm}^N(\theta', \phi') = \sum_{m'=-l}^{l} d_{mm'}^{(l)}(\beta) \mathbf{Y}_{lm'}^N(\theta, \phi) \tag{A.11}$$

where $d_{mm'}^{(l)}$ is a $(2l+1) \times (2l+1)$ real matrix. Explicit form of $d_{mm'}^{(l)}$ can be found in [4] and a python subroutine for calculating this can be found in functions.py in the Github repository [1].

Appendix B

Calculation of Sensitivity Kernels

B.1 For Differential Rotation

B.2 For Lorentz Stress

Appendix C

Fourier Convention

The following convention is employed in this work regarding temporal Fouirer transforms: